INORGANIC CHEMISTRY FRONTIERS

RESEARCH ARTICLE

View Article Online
View Journal | View Issue

Cite this: *Inorg. Chem. Front.*, 2023, **10**, 4109

$C_2O_4^{2-}$-templated cage-shaped Ln_{28} (Ln = Gd, Eu) nanoclusters with magnetocaloric effect and luminescence†

Qin Wang,[a] Sheng-Hui Lu,[a] Ling-Xi Xu,[b] Ji-Lei Wang,[a] Ya-Ting Yu,[a] Xu Bai,[a] Hua Mei[a] and Yan Xu *[a]

Received 24th April 2023,
Accepted 7th June 2023

DOI: 10.1039/d3qi00743j

rsc.li/frontiers-inorganic

The assembly of high-nuclearity lanthanide nanoclusters with favourable magnetocaloric effects suffers from a significant challenge. Herein, two outstanding examples of cage-shaped nanoclusters, namely, $[Ln_{28}(IN)_{25}(C_2O_4)_6(HCOO)(\mu_3\text{-}OH)_{36}(\mu_2\text{-}OH)_2(H_2O)_{36}]\cdot 8Br\cdot xH_2O$ (Ln = Gd and Eu; x = 21, abbreviated as **Gd$_{28}$**; x = 17, abbreviated as **Eu$_{28}$**, HIN = isonicotinic acid; $H_2C_2O_4$ = oxalic acid) have been triumphantly designed and constructed under hydrothermal conditions. The crystallographic study revealed that the aesthetically pleasing triangle-shaped **Gd$_{12}$** subunit and **Gd$_{16}$** subunit built separately from four **Gd$_3$** units and four **Gd$_4$** units, respectively, are shaped into an unprecedented cage-shaped configuration. Prominently, six small and simple $C_2O_4^{2-}$ anions generated *via* the *in situ* reaction of HIN are faultlessly anchored in the cage-shaped framework. Furthermore, the existence of abundant Gd^{III} ions impart **Gd$_{28}$** with a captivating magnetic entropy change ($-\Delta S_m^{max}$ = 37.5 J kg^{-1} K^{-1}) at 2.0 K for ΔH = 7.0 T.

Introduction

Owing to severe pollution of the environment and deficiencies from energy shortages, research on lanthanide nanoclusters with beneficial magnetocaloric effects (MCEs) has been heralded in materials chemistry and magnetochemistry.[1–7] The MCE, which explains the phenomenon of heat absorption or heat release of a magnetic material in a changing magnetic field, was first discovered in 1881 by Warburg.[8,9] In particular, magnetic cooling materials at ultra-low temperatures play an indispensable role in the development of quantum computers.[7,10–12] As a unique class of energy-efficient and environmentally friendly refrigerants at ultra-low temperatures, lanthanide nanoclusters, especially high-nuclearity Gd^{III} oxide/hydroxide clusters, are prospective materials featuring decent MCEs.[13–15] At the same time, aesthetically captivating configurations with various conformations and shapes have been designed, such as chair, boat, cage, disk, wheel, nanocapsule, *etc*.[16–21]

However, due to practical obstacles in their sizeable ionic radius and high coordination numbers, as well as the mutual repulsion between lanthanide ions, the assembly of high-nuclearity lanthanide nanoclusters is a great challenge, especially when the number of the lanthanide ions is greater than 20.[15,22,23] It is well known that *in situ* reactions can benefit the formation of anionic templates through decomposition, rearrangement and other unpredictable side reactions of solvents or ligands.[24] Once an *in situ* reaction occurs, the decomposition of ligands can effectively realize the slow release of anions. The decomposition process is pretty slow, thus avoiding the formation of precipitation caused by the direct introduction of raw materials, which makes the sophisticated coordination mode possible.[25,26] For example, the synthesis of classical cage-like **Ln$_{60}$** is through the *in situ* reaction of 2,2′-bipyridine-4,4′-dicarboxylic acid, where the small and simple carbonate anion is resoundingly encapsulated in the nanocluster. The synthesis of stable and compact inorganic–organic hybrid **Gd$_4$** with twisted cubic $[Gd_4O_4]$ units is bridged by *in situ* generated oxalate and sulfate.[27,28] So far, it has been observed that ligands containing carboxylic acid, an N-donor or sulfur tend to react *in situ*.[29,30] Indeed, pyridinecarboxylate acids, such as isonicotinic acid, may be converted into some small ligands *via* an *in situ* reaction to form into exquisite frameworks with large MCEs. As a result, the first mixed-ligand (oxalate and isonicotinic acid) coordination polymer $[Zn_2(IN)_2(oxa)]$ was afforded under hydrothermal conditions from the *in situ* reaction of HIN to oxalate. Subsequently, a 3D compound of $[La_2(C_2O_4)_2]$ was reported under hydrothermal conditions from the *in situ* reaction of HIN.[31,32] Although HIN can be chemically rearranged to oxalate under appropriate con-

[a]*College of Chemical Engineering, State Key Laboratory of Materials-Oriented Chemical Engineering, Nanjing Tech University, Nanjing 211816, P. R. China. E-mail: yanxu@njtech.edu.cn*
[b]*College of Software, Jilin University, Changchun 130012, P. R. China*

†Electronic supplementary information (ESI) available. CCDC 2257351. For ESI and crystallographic data in CIF or other electronic format see DOI: https://doi.org/10.1039/d3qi00743j

ditions, it has never been observed in high-nuclearity lanthanide nanoclusters.

Based on the high-nuclearity lanthanide nanoclusters of **Ln_{26}** (Ln = Ho and Er) and **Ho_{48}** by employing isonicotinic acid as the ligand, we elaborately designed and isolated two unprecedented cage-shaped nanoclusters under hydrothermal conditions with the formulas of $[Gd_{28}(IN)_{25}(C_2O_4)_6(HCOO)(\mu_3\text{-}OH)_{36}(\mu_2\text{-}OH)_2(H_2O)_{36}]\cdot 8Br\cdot 21H_2O$ and $[Eu_{28}(IN)_{25}(C_2O_4)_6(HCOO)(\mu_3\text{-}OH)_{36}(\mu_2\text{-}OH)_2(H_2O)_{36}]\cdot 8Br\cdot 17H_2O$.[20,33] Structural analysis showed that the aesthetically elegant cage-shaped **Gd_{28}** can be divided into the charming triangle-shaped **Gd_{12}** subunit and the triangle-shaped **Gd_{16}** subunit that are constructed from four **Gd_3** units and four **Gd_4** units, respectively. Remarkably, the small and simple $C_2O_4^{2-}$ anion generated *via* the *in situ* reaction of HIN is splendidly anchored in the cage-shaped framework, which is the first case in the family of high-nuclearity lanthanide nanoclusters. Besides, magnetocaloric analysis showed that **Gd_{28}** exhibited a considerable value of $-\Delta S_m^{max} = 37.5$ J kg^{-1} K^{-1} at 2.0 K for $\Delta H = 7.0$ T.

Experimental section

Materials and physical measurements

Chemical raw solvents and reagents from commercial sources were available for use without further purification. A PerkinElmer 2400 analyzer (USA) was used for the elemental analyses of C, H, and N. A Bruker D8 diffractometer (Germany) was used to collect powder X-ray diffraction (PXRD) data using Cu Kα radiation (λ = 1.5418 Å) in the 2θ range of 3–50° at a scanning rate of 3° min^{-1} at room temperature. IR spectra of the two compounds in KBr pellets were recorded using a Nicolet Impact 410 spectrometer (Thermo Fisher, USA) in the region of 4000–400 cm^{-1}. In order to conduct a thermogravimetric analysis (TGA), a Q50 Thermogravimetric Analyzer (TA Instruments, USA) was used in flowing nitrogen air to record thermogravimetric curves of the two compounds from ambient temperature to 1000 °C at a rate of 10 °C min^{-1}. The energy dispersive spectrometry (EDS) data were acquired with a Hitachi S-4800 (Japan) emission scanning electron microscope with a 20 kV accelerating voltage. Magnetization measurements were performed using an MPMS-XL7 SQUID magnetometer (Quantum Design, USA) at 1.8–300 K and in fields of 0–7 T. The solid-state luminescence properties of **Eu_{28}** were measured using an FLS1000 spectrophotometer (Edinburgh Instruments, UK) at room temperature.

X-ray crystallography

Under an optical microscope, single crystals of **Gd_{28}** with good crystal quality were selected and coated quickly with epoxy glue in air, and placed on a thin glass fiber for data collection; the crystal data of **Eu_{28}** were not good enough to be reported in detail. Single crystal X-ray diffraction (SCXRD) data of **Gd_{28}** were collected by employing a Bruker Apex II CCD (Germany) with a sealed-tube X-ray source in the ω–2θ scanning method at room temperature. The SHELX software package was used to resolve the crystal structures with direct methods and refine the crystal structures *via* full-matrix least-squares approaches. Besides, all the non-hydrogen atoms were refined by using anisotropic thermal parameters according to experience. The H atoms of water were not located. The SQUEEZE command was used to remove the H_2O molecules. Table 1 provides the relevant crystal data. Table S5† shows the selected bond lengths and angles.

Synthesis of Gd_{28}

The reactants of HIN (0.25 g, 2.00 mmol), Gd_2O_3 (0.20 g, 0.55 mmol), Al_2O_3 (0.04 g, 0.39 mmol) and KBr (0.01 g, 0.08 mmol) were placed in a 25 mL Teflon-lined autoclave, to which were added HCOOH (0.04 g, 0.87 mmol) and 8 mL of distilled water. Immediately after, the mixture was magnetically stirred at room temperature for 12 hours, and then the pH was adjusted from 4.8 to 2.0 with HNO_3 (50%) under stirring conditions. Subsequently, the mixture was maintained at 170 °C for 7 days. After cooling to about room temperature, light-yellow quadrilateral crystals were harvested (as shown in Fig. S1†), which were washed with distilled water (37.0% yield based on Gd). Anal. calcd (%) for $C_{163}H_{253}Gd_{28}N_{25}O_{171}Br_8$ (formula weight = 10 341): C, 18.93; H, 2.45; N, 3.39. Found: C, 18.90; H, 2.41; N, 3.40.

Synthesis of Eu_{28}

The synthesis method is the same as the method used for **Gd_{28}** except for Gd_2O_3 being replaced with Eu_2O_3. The light-yellow quadrilateral crystals were obtained (as shown in Fig. S1†) (35% yield based on Eu). Anal. calcd (%) for

Table 1 Crystal data and structure refinements for **Gd_{28}**

Compound	**Gd_{28}**
Formula	$C_{163}H_{253}Gd_{28}N_{25}O_{171}Br_8$
Formula weight	10 341
T (K)	296(2)
Crystal system	Triclinic
Space group	$P\bar{1}$
a (Å)	21.465(5)
b (Å)	24.112(5)
c (Å)	30.492(6)
α (°)	87.190(3)
β (°)	79.559(3)
γ (°)	88.080(3)
V (Å^3)	15 496(6)
Z	2
D_c (mg m^{-3})	2.216
μ (mm^{-1})	7.027
F (000)	9692
θ range (°)	0.680–27.322
Limiting indices	$-26 \le h \le 27$, $-30 \le k \le 29$, $-38 \le l \le 36$
Reflections collected	123 261
R(int)	0.0611
Data/restraints/parameters	61 613/852/3297
GOF	1.013
R_1[a], wR_2[b] [$I > 2\sigma(I)$]	$R_1 = 0.0496$, w$R_2 = 0.1353$
R_1, wR_2 (all data)	$R_1 = 0.1085$, w$R_2 = 0.1586$

[a] $R_1 = \sum||F_o| - |F_c||/\sum|F_o|$. [b] $wR_2 = \sum[w(F_o^2 - F_c^2)^2]/\sum[w(F_o^2)^2]^{1/2}$.

$C_{163}H_{245}Eu_{28}N_{25}O_{167}Br_8$ (formula weight = 10 269): C, 19.07; H, 2.40; N, 3.41. Found: C, 19.09; H, 2.37; N, 3.40.

Results and discussion

Synthetic description

The nearly light-yellow quadrilateral crystals of **Gd_{28}** were synthesized using the hydrothermal reaction of Gd_2O_3, Al_2O_3, HIN and KBr in the presence of HCOOH at 170 °C for seven days. Notably, the reagent isonicotinic acid with both an O-donor and an N-donor on opposite sides is exceptionally significant in the self-assembly of the **Gd_{28}** nanocluster. Furthermore, the target product could not be captured when we tried to add oxalic acid directly to the reaction. Due to the slow production of $C_2O_4^{2-}$ anions in the *in situ* reaction of isonicotinic acid, the environment can self-adjust to realize the balance between the Gd^{III} ions, $C_2O_4^{2-}$ anions and HIN ligands, resulting in the assembly of the **Gd_{28}** nanocluster in the method of slow crystallization.[15] According to the literature, formic acid (HCOOH), as the smallest carboxylate ligand, has been favourably used to prepare lanthanide clusters with great MCEs. Gd_2O_3 is a reactant which not only can slowly release Gd^{III} ions but also regulates the pH of the reaction system. Although Al^{III} ions are not involved in the final construction, we cannot obtain the target product without them. We replaced Al_2O_3 with other metallic oxides, such as Fe_2O_3 or Cr_2O_3, but we did not get the target crystal. At the same time, we tried using Eu_2O_3, Tb_2O_3 or Dy_2O_3 instead of Gd_2O_3; only from the environment of Eu_2O_3 were light-yellow quadrilateral crystals of **Eu_{28}** isolated, but unfortunately, the crystal data were not good enough to be reported in detail. On the other hand, the synthetic process of high-nuclearity Ln-exclusive nanoclusters is problematic and heavily relies on certain reaction factors, such as reaction conditions (duration, temperature, pH, cooling rate) and reactants (solvents, ligands, and the kinds of anions). For **Gd_{28}**, a temperature of 170 °C plays a remarkable role in the formation of the framework; no crystals can be obtained at 160 °C or 140 °C. Most importantly, an absolutely acidic environment (pH = 2) is quite prominent in the self-assembly of the structure, where no crystals can be obtained at pH = 3, pH = 4 or pH = 5. The high temperature and acidic conditions make it possible for the slow release or production of $C_2O_4^{2-}$ ions from HIN.

Crystal structure

Counterions were confirmed *via* EDS analyses and charge balance studies, while the guest molecules were determined by elemental analysis, and TG and IR measurements. Data from SCXRD analysis revealed that **Gd_{28}** crystallized in a triclinic crystal system, with $P\bar{1}$ space group. As shown in Fig. 1a, the isolated nanocluster with formula $[Gd_{28}(IN)_{25}(C_2O_4)_6(HCOO)(\mu_3\text{-}OH)_{36}(\mu_2\text{-}OH)_2(H_2O)_{36}]$ can be viewed as being constructed from a 28-metal nanocage of $[Gd_{28}(C_2O_4)_6(\mu_3\text{-}OH)_{36}(\mu_2\text{-}OH)_2]^{34+}$ protected and stabilized by 25 IN^- groups, one $HCOO^-$ group and about 36 guest water molecules. Broadly, six small and

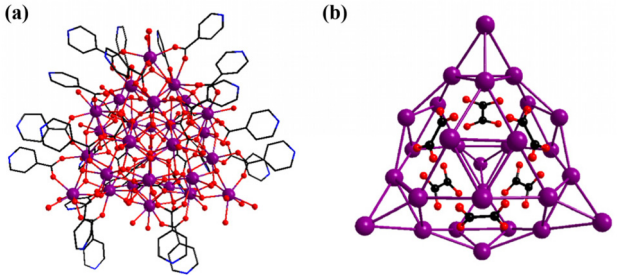

Fig. 1 (a) Plot of the whole molecular structure and (b) the $C_2O_4^{2-}$ anion template in the metal skeleton of **Gd_{28}**. Purple, Ln; blue, N; red, O; and black, C.

simple $C_2O_4^{2-}$ anions generated *via* the *in situ* reaction of HIN are splendidly anchored in the cage-shaped metal–organic framework to balance the high positive charges and stabilize its construction (Fig. 1b).

For the sake of facilitating the description and understanding of the structural skeleton, the cage-like cationic core of **Gd_{28}** can be subdivided into two different types of primary units, *i.e.*, a triangular **Gd_3** unit formulated as $[Gd_3(\mu_3\text{-}OH)_2]^{7+}$ and a cubane-like **Gd_4** unit formulated as $[Gd_4(\mu_3\text{-}OH)_8]^{4+}$. A **$Gd_3$**-type unit, as shown in Fig. 2a, can be considered a triangular construction connected by two μ_3-OH groups and four **Gd_3** units are linked by six $C_2O_4^{2-}$ anions and formed into a $[Gd_{12}(\mu_3\text{-}OH)_8(C_2O_4)_6]^{16+}$ (**Gd_{12}**) subunit. For clarity, each of the **Gd_3** units, with a shell-shaped construction, is combined with six $C_2O_4^{2-}$ anions, and formed into a delicate triangle-like structure (Fig. 2d). A **Gd_4**-typeunit is a cubane-like configuration formed by the banding of four μ_3-OH groups, which is extremely common in other lanthanide clusters (Fig. 2c). Four **Gd_4** units are combined with the same six $C_2O_4^{2-}$ anions forming a $[Gd_{16}(\mu_3\text{-}OH)_{16}(C_2O_4)_6]^{20+}$ (**Gd_{16}**) subunit. For clarity, each tetrahedron is connected by six $C_2O_4^{2-}$ anions forming a fancy triangle-shaped framework (Fig. 2e). As shown in Fig. 2f,

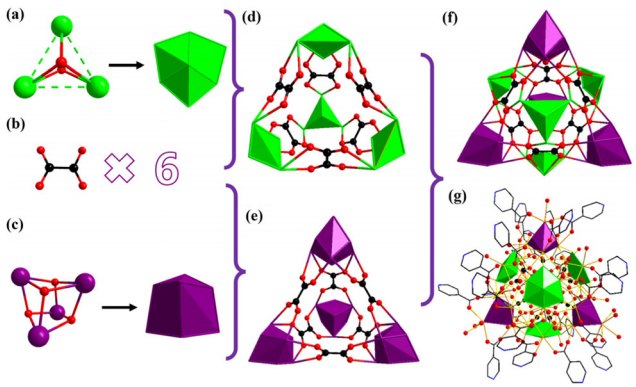

Fig. 2 Ball-and-stick views of (a) the triangular $[Gd_3(\mu_3\text{-}OH)_2]^{7+}$ unit; (b) the $C_2O_4^{2-}$ anion; (c) the cubane-like $[Gd_4(\mu_3\text{-}OH)_4]^{8+}$ unit; (d) the $[Gd_{12}(\mu_3\text{-}OH)_8(C_2O_4)_6]^{16+}$ subunit; (e) the $[Gd_{16}(\mu_3\text{-}OH)_{16}(C_2O_4)_6]^{20+}$ subunit; (f) the $[Gd_{28}(C_2O_4)_6(\mu_3\text{-}OH)_{36}(\mu_2\text{-}OH)_2]^{34+}$ nanocluster; and (g) the subunits representing **Gd_{28}**.

the frog-shaped $\mathbf{Gd_{12}}$ subunit and the frog-shaped $\mathbf{Gd_{16}}$ subunit are bonded together into an individual cage-shaped framework templated by six $C_2O_4^{2-}$ anions. The cage-like nanocluster is further stabilized by the 25 IN^- groups and one $HCOO^-$ group. Additionally, the IN^- ligands in $\mathbf{Gd_{28}}$ display three different types of coordination modes, μ_2-η^1:η^0:η^1, μ_1-η^0:η^0:η^1 and μ_1-η^1:η^0:η^1 (Fig. 3a), and the six $C_2O_4^{2-}$ anions exhibit only one coordination mode, μ_6-η^2:η^2:η^2:η^2 (Fig. 3b).

The metal framework of $\mathbf{Gd_{28}}$ is shown in Fig. 1b; four tetrahedra (16 Gd^{III}) and four triangles (12 Gd^{III}) were joined together to complete the nano-caged framework. All Gd^{III} ions are located in eight-coordinated or nine-coordinated environments with different geometries (Fig. S5†). Gd3, Gd5, Gd6, Gd8, Gd11, Gd12, Gd14, Gd16, Gd25, Gd26, Gd27 and Gd28 represent eight coordination modes in the [GdO_8] polyhedra; Gd1, Gd2, Gd4, Gd7, Gd9, Gd10, Gd13, Gd15, Gd17, Gd18, Gd19, Gd20, Gd21, Gd22, Gd23 and Gd24 display nine coordination modes in the [GdO_9] polyhedra. As shown in Fig. S5,† 28 Gd^{III} ions have different coordination environments. For example, Gd1 is coordinated with one HIN, one $C_2O_4^{2-}$ anion, four μ_3-OH groups and two coordinated water molecules. According to the continuous shape measurement (CShM) analysis, the 28 Gd^{III} ions have seven different configurations. For instance, Gd28 exhibits a twisted octa-coordinated square antiprism, while Gd10 shows a distorted nine-coordinated spherical capped square antiprism (Tables S1 and 2†). The bond lengths between two neighboring ions (Gd–O = 2.3–2.9 Å) and the bond angles between the neighboring ions (O–Gd–O = 58.8–155.3 Å) are equivalent to the previously reported Gd-based nanocluster (Table S5†).

Remarkably, cage-shaped high-nuclearity Gd-based nanoscale clusters, where the number of lanthanide ions is more than 20, are still underdeveloped. To date, only cage-shaped $\mathbf{Gd_{20}}$, $\mathbf{Gd_{26}}$, $\mathbf{Gd_{27}}$, $\mathbf{Gd_{32}}$, $\mathbf{Gd_{38}}$, $\mathbf{Gd_{50}}$, $\mathbf{Gd_{60}}$ and $\mathbf{Gd_{104}}$ nanoclusters have been reported.[18,34–37] The $\mathbf{Gd_{28}}$ nanocluster reported in this work is extraordinarily different from other reported cage-shaped nanoclusters. For example, the spherical $\mathbf{Gd_{26}}$ nanocluster consists of five cubane-like $\mathbf{Gd_4}$ units and two triangular $\mathbf{Gd_3}$ units templated by nine CO_3^{2-} anions. Nicotinic acid is the organic linker and the protective ligand in the formation of $\mathbf{Gd_{26}}$.[35] Other cage-shaped $\mathbf{Gd_{27}}$ nanoclusters

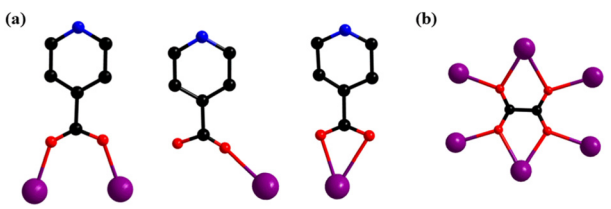

Fig. 3 Coordination modes of (a) IN^- ligands and (b) $C_2O_4^{2-}$ in $\mathbf{Gd_{28}}$.

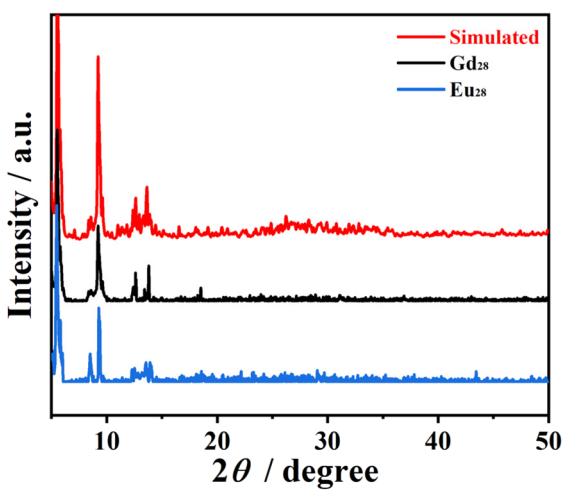

Fig. 4 PXRD patterns of $\mathbf{Gd_{28}}$ and $\mathbf{Eu_{28}}$.

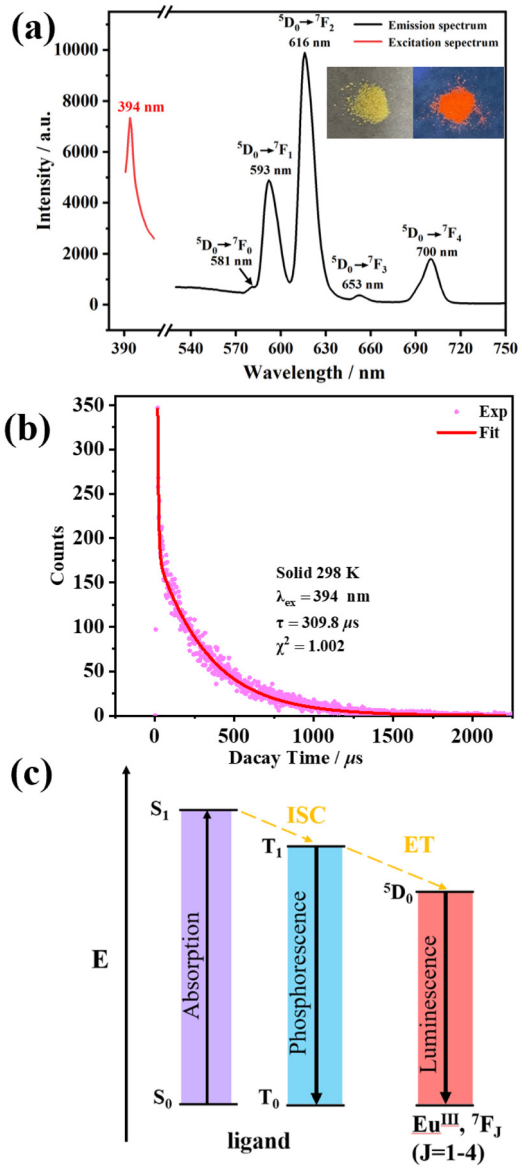

Fig. 5 (a) Excitation and emission spectra; (b) luminescence lifetime; and (c) Jablonsky level diagrams of $\mathbf{Eu_{28}}$.

have been isolated by employing sodium propionate as the ligand. The metal skeleton of $\mathbf{Gd_{27}}$ is achieved by five tetrahedral $\mathbf{Gd_4}$ units and one crown-shaped $\mathbf{Gd_7}$ unit templated by eight CO_3^{2-} anions.[18] Explicitly, the $\mathbf{Gd_{28}}$ nanocluster exhibits an unprecedented configuration in the family of high-nuclearity cage-shaped nanoclusters.

It is worth noting that the structure of the $\mathbf{Eu_{28}}$ nanocluster is roughly the same as that of $\mathbf{Gd_{28}}$, according to the main characteristic diffraction peaks of the PXRD (Fig. 4). Meanwhile, the free H_2O molecules of the two nanoclusters were determined by TG analysis, as shown in Fig. S9 and 10.† In the temperature range of 25–265 °C, the weight loss of 3.67% (calcd 3.66%) was attributed to the loss of 21 free water molecules for $\mathbf{Gd_{28}}$, while the weight loss of 2.96% (calcd 2.98%) was attributed to the loss of 17 free water molecules for $\mathbf{Eu_{28}}$.

Luminescence of $\mathbf{Eu_{28}}$

One of the most meaningful characteristics of lanthanide ions is their picturesque photoluminescence properties derived from f–f intraconfigurational transitions.[13] Additionally, Eu^{III} is most commonly used in sensing applications due to its strong visible light emission in the red region.[38] Accordingly, the luminescence properties of $\mathbf{Eu_{28}}$ with 28 Eu^{III} ions were measured at room temperature, as shown in Fig. 5. Under UV lamp irradiation, we observed the solid-state luminescence of $\mathbf{Eu_{28}}$. Besides, under maximum excitation at 394 nm, the electronic transitions of Eu^{III} from $^5D_0 \rightarrow {}^7F_J$ (J = 0, 1, 2, 3 and 4) were observed. The relatively weak emission bands at 581, 653 and 700 nm are attributed to the electronic transitions of $^5D_0 \rightarrow {}^7F_0$, $^5D_0 \rightarrow {}^7F_3$ and $^5D_0 \rightarrow {}^7F_4$, respectively. In comparison, the two sharp lines at 593 and 616 nm are assigned to the dominant electronic transitions of $^5D_0 \rightarrow {}^7F_1$ and $^5D_0 \rightarrow {}^7F_2$, respectively. Notably, the absence of a strong and broad peak from the IN^- ligand indicates the high energy transfer efficiency to the Eu^{III} center emission, known as the "antenna effect".[39] Furthermore, under the maximum excitation at 394 nm, the luminescence lifetime and the solid-state photoluminescence quantum yield (PLQY) of $\mathbf{Eu_{28}}$ were 309.8 μs and 4.18%, respectively (Fig. 5b). To further learn about the solid-state luminescence of $\mathbf{Eu_{28}}$, we drew a simple Jablonsky level diagram to explain the luminescence properties (Fig. 5c).[40–43] These findings are of significant value for understanding the optical properties of the lanthanide clusters and their applications in optoelectronic devices, among others.[44]

Magnetic properties of $\mathbf{Gd_{28}}$

At an applied direct current (dc) magnetic field of 1.0 kOe from 1.8 K to 300 K, temperature-dependent magnetic susceptibilities of $\mathbf{Gd_{28}}$ were characterized. The observed $\chi_M T$ value (225.0 cm^3 K mol^{-1}) at 300 K is slightly larger than the expected value (220.5 cm^3 K mol^{-1}) based on 28 independent Gd^{III} ions (S = 7/2, g = 2) with the Lande formula.[6] As shown in Fig. 6a, as the temperature drops from 300 K to 1.8 K, the $\chi_M T$

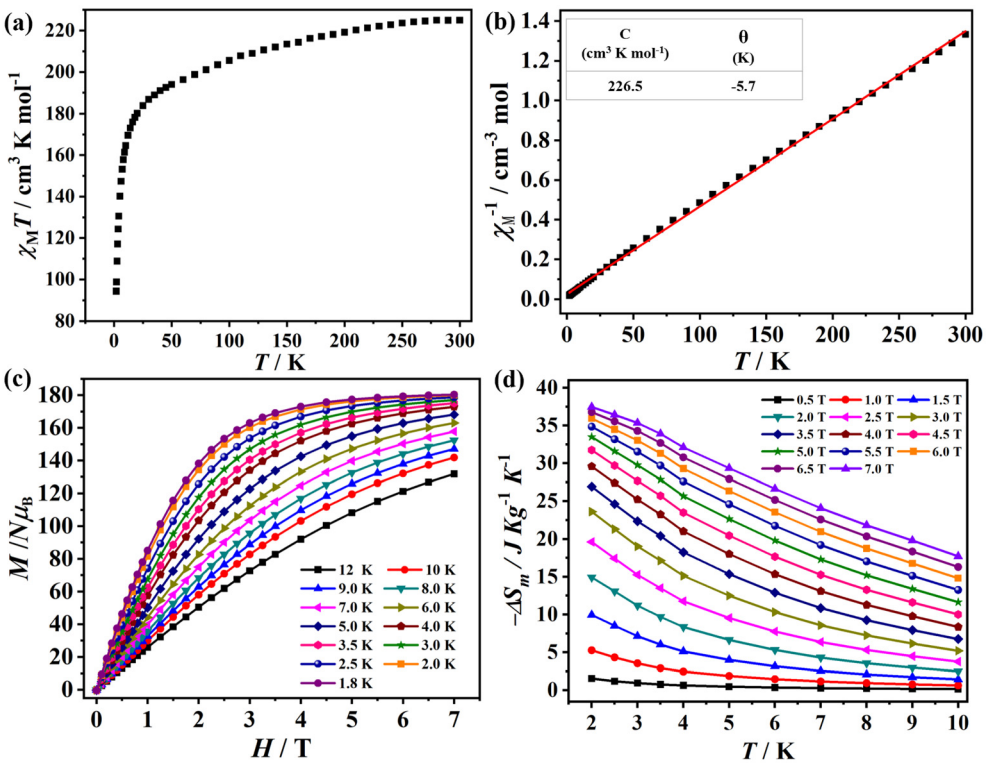

Fig. 6 (a) Plot of experimental magnetic susceptibility ($\chi_M T$) *versus* T; (b) χ_M^{-1} *versus* T plot; (c) plot of M–H under different temperatures; and (d) plot of experimental magnetic entropy change ($-\Delta S_m$) *versus* T for $\mathbf{Gd_{28}}$.

value gradually decreases to a minimum of 94.4 cm^3 K mol^{-1} at 1.8 K.[45] The overall trend of $\chi_M T$ *vs.* T data indicated that **Gd_{28}** exhibited antiferromagnetic interaction between these metal cations. At the same time, fitting the $\chi_M{}^{-1}$ *vs.* T data with the Curie–Weiss law from 1.8 K to 300 K resulted in the Weiss constant $\theta = -5.7$ K and Curie constant $C = 226.5$ cm^3 K mol^{-1}. All the above discussions demonstrate the existence of weak antiferromagnetic interactions among metal ions (Fig. 6b).[46–49]

A large number of Gd^{III} ions and fairly weak magnetic interactions between Gd^{III} ions make **Gd_{28}** nanoclusters a valid class of materials for magnetic cooling applications. Hence, it encouraged us to conduct research of the magnetocaloric effect of **Gd_{28}**. Here, the magnetization (M) and magnetic field (H) at low temperature (1.8 K–10 K) was measured (Fig. 6c). With the increase of magnetic field (H), the magnetization (M) also increased steadily to the maximum of 180.3$N\beta$ under 1.8 K and 7 T; the discrepancy between the two magnetization values (calculated value is 196.0$N\beta$ based on 28 uncorrelated metal ions) resulted from the weak antiferromagnetic interaction in the nanocluster. Subsequently, we investigated the magnetocaloric effects of **Gd_{28}** by employing the Maxwell equation of $\Delta S_m(T)_{\Delta H} = \int [\partial M(T,H)/\partial T]_H dH$ (Fig. 6d).[50] With an increased H and a reduced T, the experimental entropy changes gradually increased, and the $-\Delta S_m^{max}$ is 37.5 J kg^{-1} K^{-1} for ΔH = 7 T at 2 K. By using the equation of $-\Delta S_m = nR\ln(2S + 1)$, the 28 uncorrelated Gd^{III} ions were calculated and resulted in a theoretical value of 46.8 J kg^{-1} K^{-1}; the discrepancy between the two ΔS_m values might be due to the existence of antiferromagnetic exchanges among the metal centers.[51] As far as we know, the **Gd_{28}** nanocluster exhibits a decent magnetocaloric effect value, comparable to those of the reported high-nuclearity nanoscale clusters **Gd_{27}** ($-\Delta S_m$ = 41.8 J kg^{-1} K^{-1}), **Gd_{38}** ($-\Delta S_m$ = 37.9 J kg^{-1} K^{-1}) and **Gd_{36}** ($-\Delta S_m$ = 39.7 J kg^{-1} K^{-1}), validating its excellent potential application in magnetic cooling (Table S3†).[18,36,52]

Conclusions

In summary, we triumphantly obtained two novel high-nuclearity lanthanide nanoclusters **Gd_{28}** and **Eu_{28}** in the presence of HIN under hydrothermal conditions. Subsequently, through structural characterization studies, we observed that the charming triangle-shaped **Gd_{12}** subunit and **Gd_{16}** subunit assembled by four **Gd_3** units and four **Gd_4** units, respectively, were arranged into an unprecedented cage-shaped structure featuring six $C_2O_4{}^{2-}$ anions. Notably, this is the first case of an *in situ* hydrolysis of isonicotinic acid to $C_2O_4{}^{2-}$ ions in constructing high-nuclearity lanthanide nanoclusters. Magnetization analysis revealed that **Gd_{28}** exhibits a decent magnetocaloric effect of 37.5 J kg^{-1} K^{-1} at 2.0 K for ΔH = 7.0 T. This paper has given a new idea for introducing $C_2O_4{}^{2-}$ from the *in situ* reaction of HIN to assemble high-nuclearity lanthanide clusters with large magnetic entropy changes. Next, we will continue to isolate molecular magnetocaloric materials based on Gd nanoclusters through the *in situ* hydrolysis of HIN and probe more excellent properties and potential applications for high-nuclearity lanthanide clusters.

Conflicts of interest

The authors declare no competing financial interest.

Acknowledgements

This work was supported by the Natural Science Foundation of China (Grant 92161109).

References

1 W. P. Chen, P. Q. Liao, Y. Yu, Z. Zheng, X. M. Chen and Y. Z. Zheng, A Mixed-Ligand Approach for a Gigantic and Hollow Heterometallic Cage $\{Ni_{64}RE_{96}\}$ for Gas Separation and Magnetic Cooling Applications, *Angew. Chem., Int. Ed.*, 2016, **55**, 9375–9379.
2 N. F. Li, Q. F. Lin, Y. M. Han, Z. Y. Du and Y. Xu, The chain-shaped coordination polymers based on the bowl-like $Ln_{18}Ni_{24}(_{23.5})$ clusters exhibiting favorable low-field magnetocaloric effect, *Chin. Chem. Lett.*, 2021, **32**, 3803–3806.
3 N. F. Li, Q. F. Lin, X. M. Luo, J. P. Cao and Y. Xu, Cl^--Templated Assembly of Novel Peanut-like $Ln_{40}Ni_{44}$ Heterometallic Clusters Exhibiting a Large Magnetocaloric Effect, *Inorg. Chem.*, 2019, **58**, 10883–10889.
4 E. Moreno Pineda, F. Tuna, R. G. Pritchard, A. C. Regan, R. E. Winpenny, E. J. McInnes and Y. Z. Zheng, Molecular amino-phosphonate cobalt-lanthanide clusters, *Chem. Commun.*, 2013, **49**, 3522–3524.
5 J. B. Peng, Q. C. Zhang, X. J. Kong, Y. Z. Zheng, Y. P. Ren, L. S. Long, R. B. Huang, L. S. Zheng and Z. Zheng, High-nuclearity 3d-4f clusters as enhanced magnetic coolers and molecular magnets, *J. Am. Chem. Soc.*, 2012, **134**, 3314–3317.
6 Z. X. Lu, Z. Zhuo, W. Wang, Y. G. Huang and M. C. Hong, $\{Gd_{44}Ni_{22}\}$: a gigantic 3d–4f wheel-like nanoscale cluster with a large magnetocaloric effect, *Inorg. Chem. Front.*, 2023, **10**, 979–983.
7 J. L. Wang, M. X. Yang, N. F. Li, X. M. Liu, J. N. Li, Q. D. Ping and Y. Xu, Two Ni-Substituted Trilacunary Keggin-Type Polyoxometalates: Syntheses, Crystal Structures, NLO Studies, and Magnetic Properties, *Inorg. Chem.*, 2021, **60**, 13748–13755.
8 E. Warburg, Magnetische Untersuchungen, *Ann. Phys.*, 1881, **249**, 141–164.
9 N. F. Li, Q. Wang, J. N. Li, Y. T. Yu and Y. Xu, Two $SiO_4{}^{4-}$-Templated $Ln_{23}Ni_{20}$ Clusters with Magnetic Cooling and Stability, *Inorg. Chem.*, 2022, **61**, 7180–7187.
10 Y. Zheng, Q. C. Zhang, L. S. Long, R. B. Huang, A. Muller, J. Schnack, L. S. Zheng and Z. Zheng, Molybdate templated assembly of $Ln_{12}Mo_4$-type clusters (Ln = Sm, Eu, Gd) con-

taining a truncated tetrahedron core, *Chem. Commun.*, 2013, **49**, 36–38.

11 Y. Z. Zheng, E. M. Pineda, M. Helliwell and R. E. Winpenny, Mn^{II}-Gd^{III} phosphonate cages with a large magnetocaloric effect, *Chem. – Eur. J.*, 2012, **18**, 4161–4165.

12 J. J. Hu, Y. Peng, S. J. Liu and H. R. Wen, Recent advances in lanthanide coordination polymers and clusters with magnetocaloric effect or single-molecule magnet behavior, *Dalton Trans.*, 2021, **50**, 15473–15487.

13 Q. Wang, Y. T. Yu, J. L. Wang, J. N. Li, N. F. Li, X. Fan and Y. Xu, Two Windmill-Shaped Ln_{18} Nanoclusters Exhibiting High Magnetocaloric Effect and Luminescence, *Inorg. Chem.*, 2023, **62**, 3162–3169.

14 J.-L. Liu, Y.-C. Chen, F.-S. Guo and M.-L. Tong, Recent advances in the design of magnetic molecules for use as cryogenic magnetic coolants, *Coord. Chem. Rev.*, 2014, **281**, 26–49.

15 X. Y. Zheng, X. J. Kong, Z. Zheng, L. S. Long and L. S. Zheng, High-Nuclearity Lanthanide-Containing Clusters as Potential Molecular Magnetic Coolers, *Acc. Chem. Res.*, 2018, **51**, 517–525.

16 J. Hao, L. Geng, J. Zheng, J. Wei, L. Zhang, R. Feng, J. Zhao, Q. Li, J. Pang and X. H. Bu, Ligand Induced Double-Chair Conformation Ln_{12} Nanoclusters Showing Multifunctional Magnetic and Proton Conductive Properties, *Inorg. Chem.*, 2022, **61**, 3690–3696.

17 J. N. Li, N. F. Li, J. L. Wang, X. M. Liu, Q. D. Ping, T. T. Zang, H. Mei and Y. Xu, A new family of boat-shaped Ln_8 clusters exhibiting the magnetocaloric effect and slow magnetic relaxation, *Dalton Trans.*, 2021, **50**, 13925–13931.

18 X. Y. Zheng, J. B. Peng, X. J. Kong, L. S. Long and L. S. Zheng, Mixed-anion templated cage-like lanthanide clusters: Gd_{27} and Dy_{27}, *Inorg. Chem. Front.*, 2016, **3**, 320–325.

19 J. M. Peng, H. L. Wang, Z. H. Zhu, J. Bai, F. P. Liang and H. H. Zou, Series of the Largest Dish-Shaped Dysprosium Nanoclusters Formed by In Situ Reactions, *Inorg. Chem.*, 2022, **61**, 6094–6100.

20 L. Chen, J. Y. Guo, X. Xu, W. W. Ju, D. Zhang, D. R. Zhu and Y. Xu, A novel 2-D coordination polymer constructed from high-nuclearity waist drum-like pure Ho_{48} clusters, *Chem. Commun.*, 2013, **49**, 9728–9730.

21 L. X. Chang, G. Xiong, L. Wang, P. Cheng and B. Zhao, A 24-Gd nanocapsule with a large magnetocaloric effect, *Chem. Commun.*, 2013, **49**, 1055–1057.

22 Z.-R. Luo, H. L. Wang, Z. H. Zhu, T. Liu, X. F. Ma, H. F. Wang, H. H. Zou and F. P. Liang, Assembly of Dy_{60} and Dy_{30} cage-shaped nanoclusters, *Commun. Chem.*, 2020, **3**, 30–36.

23 W. Q. Lin, X. F. Liao, J. H. Jia, J. D. Leng, J. L. Liu, F. S. Guo and M. L. Tong, Lanthanide oxide clusters: from tetrahedral $[Dy_4(\mu_4\text{-}O)]^{10+}$ to supertetrahedral $[Ln_{20}(\mu_4\text{-}O)_{11}]^{38+}$ (Ln = Tb, Dy, Ho, Er), *Chem. – Eur. J.*, 2013, **19**, 12254–12258.

24 S. J. Liu, S. D. Han, J. P. Zhao, J. Xu and X. H. Bu, *In situ* synthesis of molecular magnetorefrigerant materials, *Coord. Chem. Rev.*, 2019, **394**, 39–52.

25 J. Xu, W. Su and M. Hong, 3D lanthanide–transition-metal–organic frameworks constructed from tetranuclear $\{Ln_4\}$ SBUs and Cu centres with fsc net, *CrystEngComm*, 2011, **13**, 3998–4004.

26 X. Y. Zheng, S. Q. Wang, W. Tang, G. L. Zhuang, X. J. Kong, Y. P. Ren, L. S. Long and L. S. Zheng, Two nanosized 3d-4f clusters featuring four Ln_6 octahedra encapsulating a Zn_4 tetrahedron, *Chem. Commun.*, 2015, **51**, 10687–10690.

27 X. M. Luo, Z. B. Hu, Q. F. Lin, W. Cheng, J. P. Cao, C. H. Cui, H. Mei, Y. Song and Y. Xu, Exploring the Performance Improvement of Magnetocaloric Effect Based Gd-Exclusive Cluster Gd_{60}, *J. Am. Chem. Soc.*, 2018, **140**, 11219–11222.

28 S.-D. Han, X. H. Miao, S. J. Liu and X. H. Bu, Magnetocaloric effect and slow magnetic relaxation in two dense (3,12)-connected lanthanide complexes, *Inorg. Chem. Front.*, 2014, **1**, 549–552.

29 P. F. Shi, Y. Z. Zheng, X. Q. Zhao, G. Xiong, B. Zhao, F. F. Wan and P. Cheng, 3 D MOFs containing trigonal bipyramidal Ln_5 clusters as nodes: large magnetocaloric effect and slow magnetic relaxation behavior, *Chem. – Eur. J.*, 2012, **18**, 15086–15091.

30 S. Zhang, E. Duan and P. Cheng, An exceptionally stable 3D GdIII-organic framework for use as a magnetocaloric refrigerant, *J. Mater. Chem. A*, 2015, **3**, 7157–7162.

31 L. Z. Zhang, W. Gu, B. Li, X. Liu and D. Z. Liao, $\{[Nd_4(ox)_4(NO_3)_2(OH)_2(H_2O)_2]\cdot 5H_2O\}n$: A Porous 3D Lanthanide-Based Coordination Polymer with a Special Luminescent Property, *Inorg. Chem.*, 2007, **46**, 622–624.

32 J. Y. Lu, J. Macias, J. Lu and J. E. Cmaidalka, An Unforeseen Chemical Rearrangement of Pyridine carboxylate to Oxalate under Hydrothermal Conditions Afforded the First Oxalato and Isonicotinato Mixed-Ligand Guest-Inclusion Coordination Polymer, *Cryst. Growth Des.*, 2002, **2**, 485–487.

33 L. Chen, L. Huang, C. Wang, J. Fu, D. Zhang, D. Zhu and Y. Xu, Hydrothermal synthesis, structure, and properties of two new nanosized Ln26 (Ln=Ho, Er) clusters, *J. Coord. Chem.*, 2012, **65**, 958–968.

34 L. Qin, G. J. Zhou, Y. Z. Yu, H. Nojiri, C. Schroder, R. E. P. Winpenny and Y. Z. Zheng, Topological Self-Assembly of Highly Symmetric Lanthanide Clusters: A Magnetic Study of Exchange-Coupling "Fingerprints" in Giant Gadolinium(III) Cages, *J. Am. Chem. Soc.*, 2017, **139**, 16405–16411.

35 R. Sen, D. K. Hazra, M. Mukherjee and S. Koner, Gd_{26} Cluster Consisting of Distorted Cubane Cores: Synthesis, Structure and Heterogeneous Catalytic Epoxidation of Olefins, *Eur. J. Inorg. Chem.*, 2011, **2011**, 2826–2831.

36 F. S. Guo, Y. C. Chen, L. L. Mao, W. Q. Lin, J. D. Leng, R. Tarasenko, M. Orendac, J. Prokleska, V. Sechovsky and M. L. Tong, Anion-templated assembly and magnetocaloric properties of a nanoscale $\{Gd_{38}\}$ cage versus a $\{Gd_{48}\}$ barrel, *Chem. – Eur. J.*, 2013, **19**, 14876–14885.

37 J. B. Peng, X. J. Kong, Q. C. Zhang, M. Orendac, J. Prokleska, Y. P. Ren, L. S. Long, Z. Zheng and

L. S. Zheng, Beauty, symmetry, and magnetocaloric effect-four-shell keplerates with 104 lanthanide atoms, *J. Am. Chem. Soc.*, 2014, **136**, 17938–17941.

38 T. Q. Lu, H. Xu, L. T. Cheng, X. T. Wang, C. Chen, L. Cao, G. L. Zhuang, J. Zheng and X. Y. Zheng, Family of Nanoclusters, Ln33 (Ln = Sm/Eu) and Gd32, Exhibiting Magnetocaloric Effects and Fluorescence Sensing for MnO4^{-}, *Inorg. Chem.*, 2022, **61**, 8861–8869.

39 Y. L. Li, H. L. Wang, Z. C. Chen, Z. H. Zhu, Y. C. Liu, R. Y. Yang, F. P. Liang and H. H. Zou, Lanthanoid hydrogen-bonded organic frameworks: Enhancement of luminescence by the coordination-promoted antenna effect and applications in heavy-metal ion sensing and sterilization, *Chem. Eng. J.*, 2023, **451**, 138880.

40 H. F. Wang, X. F. Ma, Z. H. Zhu, H. H. Zou and F. P. Liang, Regulation of the Metal Center and Coordinating Anion of Mononuclear Ln(III) Complexes to Promote an Efficient Luminescence Response to Various Organic Solvents, *Langmuir*, 2020, **36**, 1409–1417.

41 H. F. Wang, Z. H. Zhu, J. M. Peng, B. Yin, H. L. Wang, H. H. Zou and F. P. Liang, Multifunctional Binuclear Ln(III) Complexes Obtained via In Situ Tandem Reactions: Multiple Photoresponses to Volatile Organic Solvents and Anticounterfeiting and Magnetic Properties, *Inorg. Chem.*, 2020, **59**, 13774–13783.

42 J. Zhou, H. Li, H. Zhang, H. Li, W. Shi and P. Cheng, A Bimetallic Lanthanide Metal-Organic Material as a Self-Calibrating Color-Gradient Luminescent Sensor, *Adv. Mater.*, 2015, **27**, 7072–7077.

43 S. S. Sun, Z. Wang, X. W. Wu, J. H. Zhang, C. J. Li, S. Y. Yin, L. Chen, M. Pan and C. Y. Su, ESIPT-Modulated Emission of Lanthanide Complexes: Different Energy-Transfer Pathways and Multiple Responses, *Chem. – Eur. J.*, 2018, **24**, 10091–10098.

44 P.-Da Liu, Ao.-G. Liu, P.-M. Wang, Y. Chen and B. Li, Smart crystalline frameworks constructed with bisquinoxaline-based component for multi-stimulus luminescent sensing materials, *Chin. J. Struct. Chem.*, 2023, **42**, 100001.

45 W. P. Chen, P. Q. Liao, P. B. Jin, L. Zhang, B. K. Ling, S. C. Wang, Y. T. Chan, X. M. Chen and Y. Z. Zheng, The Gigantic {$Ni_{36}Gd_{102}$} Hexagon: A Sulfate-Templated "Star-of-David" for Photocatalytic CO_2 Reduction and Magnetic Cooling, *J. Am. Chem. Soc.*, 2020, **142**, 4663–4670.

46 F. Shao, J. J. Zhuang, M. G. Chen, N. Wang, H. Y. Shi, J. P. Tong, G. Luo, J. Tao and L. S. Zheng, Facile and environmentally friendly synthesis of six heterometallic dumbbell-shaped MLn (M = Co, Ni; Ln = Eu, Gd, Dy) clusters as cryogenic magnetic coolants and molecular magnets, *Dalton Trans.*, 2018, **47**, 16850–16854.

47 M. H. Du, D. H. Wang, L. W. Wu, L. P. Jiang, J. P. Li, L. S. Long, L. S. Zheng and X. J. Kong, Hierarchical Assembly of Coordination Macromolecules with Atypical Geometries: Gd44Co28 Crown and Gd95Co60 Cage, *Angew. Chem., Int. Ed.*, 2022, **61**, e202200537.

48 N. F. Li, Y. M. Han, J. N. Li, Q. Chen and Y. Xu, Efficiently increasing low-field magnetic entropy by incorporating SO_3^{2-} into $Gd_{22}Ni_{21}$ clusters, *Dalton Trans.*, 2022, **51**, 2669–2673.

49 P. Hu, S. Li, L. Cao, A. Liu, G. L. Zhuang, L. Ji and B. Li, Construction of a High Nuclear Gadolinium Cluster with Enhanced Magnetocaloric Effect through Structural Transition, *ACS Omega*, 2022, **7**, 38782–38788.

50 N. F. Li, X. M. Luo, J. Wang, J. L. Wang, H. Mei, Y. Song and Y. Xu, Largest 3d-4f 196-nuclear $Gd_{158}Co_{38}$ clusters with excellent magnetic cooling, *Sci. China: Chem.*, 2022, **65**, 1577–1583.

51 R. Chen, C. L. Chen, M. H. Du, X. Wang, C. Wang, L. S. Long, X. J. Kong and L. S. Zheng, Soluble lanthanide-transition-metal clusters $Ln_{36}Co_{12}$ as effective molecular electrocatalysts for water oxidation, *Chem. Commun.*, 2021, **57**, 3611–3614.

52 M. Y. Wu, F. L. Jiang, X. J. Kong, D. Q. Yuan, L. S. Long, S. A. Al-Thabaiti and M. C. Hong, Two polymeric 36-metal pure lanthanide nanosize clusters, *Chem. Sci.*, 2013, **4**, 3104–3109.

